Modelling mass transfer in a rotating disk reaction vessel

Problem presented by

Frank Chang and Mustapha Abbad

Schlumberger Carbonate Research Dhahran

Executive Summary

A rotating disk apparatus is commonly used to study kinetics of heterogeneous reactions such as calcite dissolution by acid. The apparatus consists of a rock disk attached to a rotating shaft; the rock is submerged in a solution of reactant which is transferred to the disk surface by convection and molecular diffusion. The former due to the rotation of the disk, and the latter due to the concentration gradient of the reactant between the bulk fluid and the rock surface.

Schlumberger is interested in determining how to use the rotating disk experiments to extract parameters that govern the reaction rate between the acid and carbonate rock. For mass transfer limited reactions these include (i) the diffusion rate across the boundary layer, and (ii) the thickness of the boundary layer. For a reaction that is surface limited, (i) the reaction rate and, (ii) the reaction order are of paramount interest.

The Study Group began by reanalyzing the solution by Levitch coupled with numerical solutions of the flow in the hope that it would lead to a deeper understanding of the fluid dynamics in the neighbourhood of the rock. In particular, how the fluid flow changes as the Reynolds number is increased and how this might indicate the most ideal location to measure the calcium in the reaction vessel.

The modelling looked not only at the coupling of the fluid flow with the diffusion equation for the ions but also a preliminary Stefan problem for the dissolving rock.

Version 1.0
July 13, 2011
iii+17 pages

Report coordinator

C. Sean Bohun

Contributors

C. Sean Bohun (University of Ontario Institute of Technology, Canada)
Chris Breward (OCCAM, UK)
Mazen El-Ghoule (American University of Beirut, Lebanon)
Luiz Faria (KAUST, Saudi Arabia)
Yiannis Hadjimichael (KAUST, Saudi Arabia)
Nadeem Malik (KFUPM, Saudi Arabia)
John Norbury (OCIAM, UK)
John Ockendon (University of Oxford, UK)
Xiang Sun (KAUST, Saudi Arabia)
Jamal Uddin (University of Birmingham, UK)
Vladimir Zubkov (OCCAM, UK)

KSG 2011 was organised by
King Abdullah University of Science and Technology (KAUST)
In collaboration with
Oxford Centre for Collaborative Applied Mathematics (OCCAM)

Contents

1 Introduction

The rotating disk apparatus, as illustrated in Figure 1, is widely used in the petroleum industry to study the kinetics of heterogeneous reactions such as interfacial calcium carbonate dissolution by acid. A review of the experimental use of this device can be found in [5]. The system allows for the determination of the reaction rate, the diffusion coefficient associated with the dissolution and the order of the reaction [1, 2, 3, 9]. In practice, a carbonate rock disk is attached to a rotating shaft, and submerged in a solution of reactant (typically strong acid). The reactant is transferred to the rock surface by both convection and molecular diffusion with the overall reaction rate governed by the slower of these two processes. Much of the theory is originally due to Levitch [4], with a refinement for a large Schmidt[1] number [6], Sc, a few years later. One of the current difficulties is the significant variability in the acid reaction rate data found in reservoir rocks which is attributed to a wide variation in experimental procedure [7, 8].

In [8] a few additional factors that could lead to variations in measured results were considered. (a) As the reaction progressed the apparent dissolution rate increases due to the increase in surface area. This effect is more likely when using strong acids or elevated temperatures. (b) Highly porous rocks will indicate a more rapid dissolution rate due to the increase in surface area but in this case the laminar flow assumed on the surface of the rock may no longer be valid. (c) Clay impurities in the rock are capable of slowing the dissolution rate to as much as 25 times. Therefore some detailed mineralogy of the reservoir rock is required. (d) Acidizing additives can also have a significant effect on the observed dissolution rate.

Some of the objectives that this report will address include: (i) an evaluation of the Reynolds number effects; (ii) determination of the motion of the fluid; (iii) consideration of the concentration profile and (iv) an indication of how to extract parameters that govern the reaction rate of the dissolution process.

1.1 Experimental setup

For the experiment detailed to the Study Group, a cylindrical pellet of calcium carbonate rock, approximately 1/4 inch thick, was attached to a metal mount and submerged in the reaction vessel prior to the introduction of the reactant. A one inch gap is maintained between the surface of the fluid and the top of the reaction vessel and a pressure of 1000 psi is maintained above the fluid to keep the gaseous by-products (carbon dioxide) in solution [3]. The reactant, 1 litre of 4.4 M HCl, is injected over a period of about 30 seconds at a pressure of 3000 psi to create the 1000 psi. This occurs while the rock is spun up to the desired speed. At this time, samples are taken every minute and the concentrations of both H^+ and Ca^{2+} ions are recorded. An example of the recorded data is shown in Figure 2.

The reactant reaching the (bottom) rock surface is consumed by chemical interaction, and Schlumberger are interested in quantifying the flux R (material per

[1]The Schmidt number $\mathrm{Sc} = \frac{\mu}{\rho D_0}$ relates the relative thickness of the hydrodynamic layer and mass-transfer boundary layer.

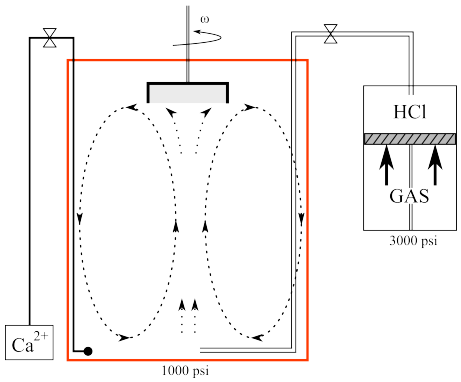

Figure 1: Experimental setup showing (i) the pump that injects concentrated acid, (ii) the rotating rock with shrink wrap exposing only the lower surface to the reactant and (iii) the sampling apparatus.

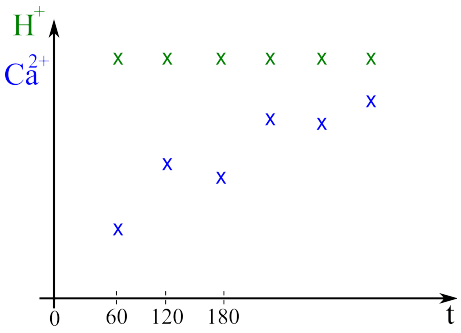

Figure 2: Experimental measurements of the hydrogen and calcium ion concentrations as a function of time in seconds.

unit area per time) of this reaction which takes the form[2] for a reaction order of $n = 1$ of

$$R = 0.62 D^{2/3} \nu^{-1/6} \omega^{1/2} (c_b - c_0) \tag{1}$$

where R is the flux from the disk surface, D is the diffusion coefficient of the solute in the solvent, $\nu = \mu/\rho$ is the kinematic viscosity, ω is the angular velocity of rotation and c_b, c_0 are the concentrations of solute in the bulk and at the disk surface respectively [4].

1.2 Schematic of flow

Measurements of the calcium concentration are taken soon after the acid is injected, without waiting for any possible transients in the ion concentrations to dissipate. In addition to this, samples from the reaction vessel were taken near the bottom of the reaction vessel against the outside wall where one would expect a recirculation cell in the fluid. Setting aside these issues, the motion of the fluid is driven by the

[2]For a general reaction order n, the industrial participant reports a generalized expression of $R = \Phi(n) D^{2/3} \nu^{-\frac{1}{3(1+n)}} R_d^{\frac{1-n}{3(1+n)}} \omega^{\frac{1}{1+n}} (c_b - c_0)$ where R_d is the radius of the pellet and $\Phi(n)$ is a constant dependent upon n.

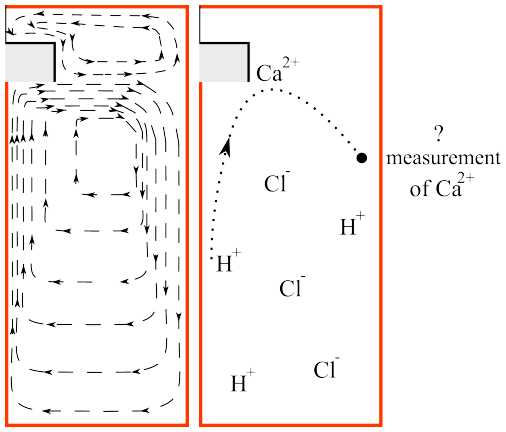

Figure 3: Schematic of the expected flow streamlines and the induced circulation of calcium ions. However, in the actual apparatus the pipes for injection and sampling disturb the axisymmetry of the flow.

spinning action of the submerged disk and in response to this motion, fluid near the disk is thrown out to the sidewall. This flow will not be axisymmetric in the flow vessel shown in Figure 1.

There is an extensive body of literature dealing with the axisymmetric flows produced by spinning disks beginning with the work of von Kármán [10] and continuing to the present [11, 12, 13]. Since the disk is submerged and is some distance from the sidewalls of the reaction vessel, it is not clear if there is a steady solution in the time frame of the experiment (5 minutes, sampling every 1 minute). Indeed, measurements in the lab have shown that occasionally $[\mathsf{Ca}^{2+}]$ decreases with time. This may be due to the location of where the $[\mathsf{Ca}^{2+}]$ is sampled. Currently this is at the bottom of the reaction vessel adjacent to the outside wall where one might expect a circulation cell in the flow. If the sampling point is within such a cell then the measurement will not be a true determination of what is occurring at the dissolution front. One of the questions that should be considered is to identify the best point to sample $[\mathsf{Ca}^{2+}]$.

Inside the reaction vessel the apparatus for sampling the fluid and injecting the reactant may complicate the structure of the flow. However, all that matters for dissolving the rock is the availability of H^+ ions through the reaction

$$2\mathsf{H}^+ + \mathsf{CaCO_3(s)} \rightleftharpoons \mathsf{Ca}^{2+} + \mathsf{CO_2(g)} + \mathsf{H_2O}.$$

If the limiting step in the dissolution is mass transfer from the rock into the solution, or the supply of hydrogen ions from the solution to the rock, then increasing the rotation speed ω would increase this mass transfer and increase the overall reaction rate. On the other hand, if the mass transfer rate exceeds the rock consumption rate then the dissolution becomes surface-reaction limited and the overall reaction rate then becomes independent of ω giving a schematic behaviour as shown in Figure 4.

A final point of concern is the effect of the bounding shrink wrap on the rock pellet. As the rock erodes, the boundary layer can become trapped by the nonreactive lip at the edge of the disk. This has the possibility of significantly changing the dynamics of the dissolution in the later stages of an experiment.

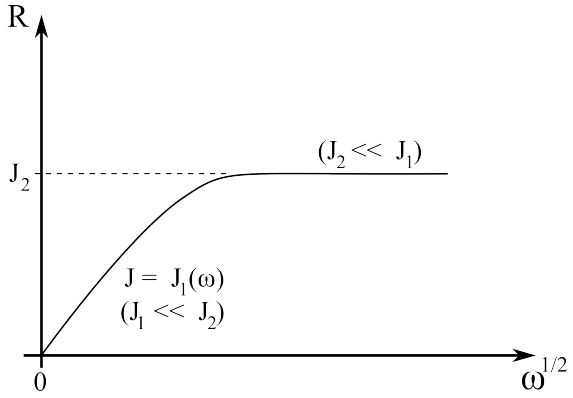

Figure 4: Schematic of the reaction rate as a function of the disk rotation speed.

2 Chemistry

2.1 The carbonic acid system

As the calcium carbonate is eaten away from the rock it injects carbonate ions into solution which react with the carbonate already present in solution due to the high pressure dissolving carbon dioxide into the solution. It is helpful to carefully quantify this chemistry before a more ambitious model is attempted.

We begin with the basic carbonic acid system where $\mathsf{CO_2(g)}$ dissolves in water to its aqueous form $\mathsf{CO_2(aq)}$ and the subsequent formation of carbonic acid. The carbonic acid decomposes into bicarbonate $\mathsf{HCO_3^-(aq)}$ and carbonate $\mathsf{CO_3^{2-}(aq)}$ ions depending upon the pH of the solution. The equilibrium system is the following

$$\mathsf{CO_2(g) + H_2O} \rightleftharpoons \mathsf{CO_2(aq) + H_2O}, \qquad K_0 = \frac{[\mathsf{CO_2(tot)}]}{P(\mathsf{CO_2})}, \tag{2a}$$

$$\mathsf{H_2CO_3(aq)} \leftrightharpoons \mathsf{H^+(aq) + HCO_3^-(aq)}, \qquad K_{a1} = \frac{[\mathsf{H^+}][\mathsf{HCO_3^-}]}{[\mathsf{CO_2(tot)}]}, \tag{2b}$$

$$\mathsf{HCO_3^-(aq)} \leftrightharpoons \mathsf{H^+(aq) + CO_3^{2-}(aq)}, \qquad K_{a2} = \frac{[\mathsf{H^+}][\mathsf{CO_3^{2-}}]}{[\mathsf{HCO_3^-}]}, \tag{2c}$$

$$\mathsf{H_2O} \leftrightharpoons \mathsf{H^+(aq) + OH^-(aq)}, \qquad K_w = [\mathsf{H^+}][\mathsf{OH^-}], \tag{2d}$$

where the notation $[\cdot]$ denotes the concentration of a particular quantity in moles/litre and $P(\cdot)$ denotes the partial pressure measured in atmospheres. The quantity $[\mathsf{CO_2(tot)}]$ denotes the concentration of the total amount of dissolved carbon dioxide which contains a small[3] admixture of dissolved carbonic acid. Values of the

[3]Carbonic acid produced with the reaction $\mathsf{CO_2(aq) + H_2O} \rightleftharpoons \mathsf{H_2CO_3(aq)}$ satisfies $[\mathsf{H_2CO_3}] = K_h[\mathsf{CO_2}]$ where $\ln K_h = -7.49 + 219/T$. At 25^o C only a small portion is converted $[\mathsf{H_2CO_3}] = 1.16 \times 10^{-3}[\mathsf{CO_2}]$.

disassociation constants are temperature dependent and given by

$$\log_{10} K_0 = 2622.38/T + 0.0178471T - 15.5873, \tag{3a}$$
$$\log_{10} K_{a1} = -3404.71/T - 0.032786T + 14.8435, \tag{3b}$$
$$\log_{10} K_{a2} = -2902.39/T - 0.02379T + 6.4980, \tag{3c}$$
$$\ln K_w = 148.9802 - 13847.26/T - 23.6521 \ln T, \tag{3d}$$

where T is the absolute temperature [14, 15, 16, 18].

Along with these reactions are expressions for both charge and mass balance. For charge balance, one ensures that $\sum_i z_i c_i = 0$ where z_i and c_i are respectively the charge and concentration of species i. This reduces to the constraint that

$$[\mathsf{H}^+] - 2[\mathsf{CO}_3^{2-}] - [\mathsf{HCO}_3^-] - [\mathsf{OH}^-] = 0. \tag{4}$$

For the mass balance, the total dissolved inorganic carbon

$$F_1 = [\mathsf{CO}_2(\mathsf{tot})] + [\mathsf{HCO}_3^-] + [\mathsf{CO}_3^{2-}] \tag{5}$$

is constant.

By combining K_{a1} and K_{a2} and using (5) one can determine the fractional amounts of the acid as a function of $[\mathsf{H}^+]$

$$\alpha_0 = \frac{1}{F_1}[\mathsf{CO}_2(\mathsf{tot})] = \frac{[\mathsf{H}^+]^2}{[\mathsf{H}^+]^2 + K_{a1}[\mathsf{H}^+] + K_{a1}K_{a2}}, \tag{6a}$$
$$\alpha_1 = \frac{1}{F_1}[\mathsf{HCO}_3^-] = \frac{K_{a1}[\mathsf{H}^+]}{[\mathsf{H}^+]^2 + K_{a1}[\mathsf{H}^+] + K_{a1}K_{a2}}, \tag{6b}$$
$$\alpha_2 = \frac{1}{F_1}[\mathsf{CO}_3^{2-}] = \frac{K_{a1}K_{a2}}{[\mathsf{H}^+]^2 + K_{a1}[\mathsf{H}^+] + K_{a1}K_{a2}}. \tag{6c}$$

To solve for $[\mathsf{H}^+]$ as a function of $P(\mathsf{CO}_2)$, expression (2) is taken with (4) to find that

$$[\mathsf{H}^+]^3 - (K_0K_{a1}P(\mathsf{CO}_2) + K_w)[\mathsf{H}^+] - 2K_0K_{a1}K_{a2}P(\mathsf{CO}_2) = 0. \tag{7}$$

Figure 5 shows the concentration of H^+, the solution to (7), as a function of the partial pressure of carbon dioxide. The black circle corresponding to an air pressure of 1 atm. At this air pressure the partial pressure of CO_2 is $P(\mathsf{CO}_2) = 39$ Pa or about 3.85×10^{-4} atm giving $[\mathsf{H}^+] = 2.41\times10^{-6}$ M (pH = 5.62). Equation (6) yields $\alpha_0 = 0.844, \alpha_1 = 0.156$ and $\alpha_2 = 3.0\times10^{-6}$ for $[\mathsf{CO}_2(\mathsf{aq})] = 1.54\times10^{-5}$ M, $[\mathsf{HCO}_3^-] = 2.41 \times 10^{-6}$ M and $[\mathsf{CO}_3^{2-}] = 4.67 \times 10^{-11}$ M. These values are reflected with the black circles in Figure 6. The squares in Figures 5, 6 correspond to an atmospheric pressure of 1000 psi or roughly 68 atm. In this case, $[\mathsf{H}^+] = 1.99 \times 10^{-5}$ M (pH = 4.70), $\alpha_0 = 0.978, \alpha_1 = 0.022$, $\alpha_2 = 5.2 \times 10^{-8}$, $[\mathsf{CO}_2(\mathsf{aq})] = 9.06 \times 10^{-4}$ M, $[\mathsf{HCO}_3^-] = 1.99 \times 10^{-5}$ M and $[\mathsf{CO}_3^{2-}] = 4.68 \times 10^{-11}$ M. As $P(\mathsf{CO}_2) \to \infty$, $[\mathsf{H}^+] \to (K_0K_{a1}P(\mathsf{CO}_2))^{1/2}$ and as a result $[\mathsf{CO}_3^{2-}] \to K_{a2}$.

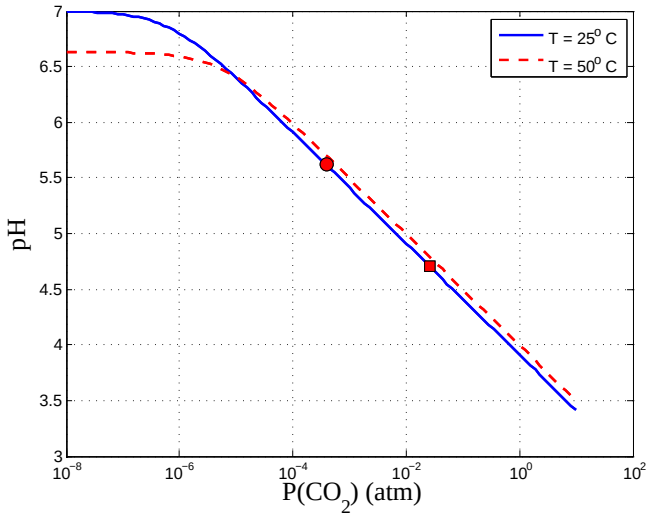

Figure 5: The dependence of the pH of a sample of pure water as a function of the applied partial pressure of carbon dioxide gas. Increasing the temperature decreases the pH at low pressures due to the change in K_w. At high pressures, pH $\sim \frac{1}{2} \log P$. The circle corresponds to an atmospheric pressure of 1 atm and the square corresponds to 1000 psi ($\sim$ 68 atm).

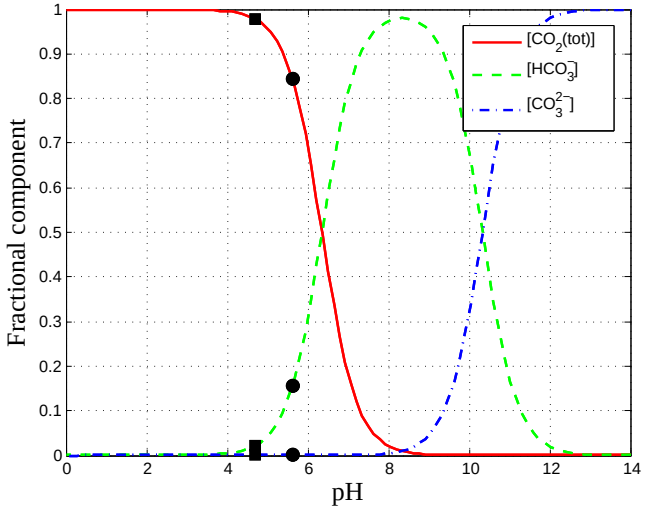

Figure 6: Fractional components of the acidic species of carbonic acid as a function of the pH of the solution at 25^{o}C. Circles correspond to a pressure of 1 atm (pH = 5.62) and squares correspond to 1000 psi ($\sim$ 68 atm) (pH = 4.70).

2.2 Solubility of calcium carbonate

In the presence of carbonate rock, the solubility depends on the amount of dissolved inorganic carbon in the water due to the applied pressure. We include the reaction

$$\mathsf{CaCO_3(s)} \rightleftharpoons \mathsf{Ca^{2+}(aq)} + \mathsf{CO_3^{2-}(aq)}, \qquad K_{\mathsf{sp}} = [\mathsf{Ca^{2+}}][\mathsf{CO_3^{2-}}] \tag{8a}$$

where

$$\log_{10} K_{\mathsf{sp}} = -171.9065 - 0.077993T + 2839.319/T - 71.595 \log_{10} T \tag{8b}$$

due to Mucci [19]. The charge balance expression becomes

$$2[\mathsf{Ca}^{2+}] + [\mathsf{H}^+] - 2[\mathsf{CO}_3^{2-}] - [\mathsf{HCO}_3^-] - [\mathsf{OH}^-] = 0. \tag{9}$$

and continuing as we did in the case of just carbonic acid, $[\mathsf{H}^+]$ satisfies

$$\begin{aligned}[\mathsf{H}^+]^3 - (K_0 K_{a1} P(\mathsf{CO}_2) + K_w)[\mathsf{H}^+] \\ -2K_0 K_{a1} K_{a2} P(\mathsf{CO}_2) = \frac{2K_{\mathsf{sp}}[\mathsf{H}^+]^4}{K_0 K_{a1} K_{a2} P(\mathsf{CO}_2)}\end{aligned} \tag{10}$$

which should be compared to (7).

It is interesting to notice what happens to the solution of (10) as $P(\mathsf{CO}_2)$ varies. At 1 atm ($P(\mathsf{CO}_2) = 3.85 \times 10^{-4}$ atm) we find the equilibrium $[\mathsf{H}^+] = 1.57 \times 10^{-7}$ M (pH = 6.80), $[\mathsf{CO}_2(\mathsf{aq})] = 1.30 \times 10^{-5}$ M, $[\mathsf{HCO}_3^-] = 3.70 \times 10^{-5}$ M, $[\mathsf{CO}_3^{2-}] = 1.11 \times 10^{-8}$ M, and $[\mathsf{Ca}^{2+}] = 4.50 \times 10^{-1}$ M. Increasing to 1000 psi (~ 68 atm) ($P(\mathsf{CO}_2) = 2.62 \times 10^{-2}$ atm), $[\mathsf{H}^+] = 1.29 \times 10^{-6}$ M (pH = 5.89), $[\mathsf{CO}_2(\mathsf{aq})] = 8.86 \times 10^{-4}$ M, $[\mathsf{HCO}_3^-] = 3.06 \times 10^{-4}$ M, $[\mathsf{CO}_3^{2-}] = 1.11 \times 10^{-8}$ M, and $[\mathsf{Ca}^{2+}] = 4.49 \times 10^{-1}$ M. Even though there is nearly 68 times the dissolved carbon in solution, the equilibrium amount of carbonate ion is virtually the same due to the buffering action of the bicarbonate ion.

In our case, the pH is controlled in that 1 litre of 4.4 M HCl is injected into the reaction vessel and if x moles of CaCO_3 dissolves, then x moles of Ca^{2+} and x moles of CO_3^{2-} are formed. The carbonate ions that are ejected into the solution will be distributed amongst the different acid forms but since we know the pH, we know that the proportion that remains as carbonate is given by α_2. That is, $K_{\mathsf{sp}} = [\mathsf{Ca}^{2+}][\mathsf{CO}_3^{2-}] = \alpha_2 x^2$ or alternatively the molar solubility is given by

$$[\mathsf{Ca}^{2+}] = \left(\frac{K_{\mathsf{sp}}}{\alpha_2([\mathsf{H}^+])}\right)^{1/2} = \left(\frac{K_{\mathsf{sp}}}{K_{a1}K_{a2}}\right)^{1/2} \left([\mathsf{H}^+]^2 + K_{a1}[\mathsf{H}^+] + K_{a1}K_{a2}\right)^{1/2}.$$

At 25^o C, a solution of 4.4 M HCl results in a massive molar solubility of $\mathsf{CaCO}_3(\mathsf{s})$ of 6.8×10^4 M.

3 Mathematical analysis

3.1 Strategy

The Study group is primarily interested in the dissolution of a carbonate rock in a rotating disk apparatus. From Section 2 it can be seen that the dissolution rate of $\mathsf{CaCO}_3(\mathsf{s})$ depends on the availability of H^+, and in a well mixed solution, the environment of the apparatus is chosen so that Ca^{2+} solubility is enhanced and the formation of CO_2 gas is suppressed. Note that the generation of CO_2 in the form of bubbles rather than in an aqueous form, can change the nature of the fluid flow.

Because the flow field is generated by a spinning disk at one end of the apparatus, it is natural to assume that, provided the flow is laminar, it will have the form of a von Kármán similarity solution. However, there are some significant differences

Description	Symbol	Value	
Depth of the top of the rotating mount	L_0	1.5×10^{-2}	m
Depth of the rock face	L_d	3.0×10^{-2}	m
Total depth of the reaction vessel	L_c	2.3×10^{-1}	m
Radius of the reaction vessel	R_c	7.5×10^{-2}	m
Radius of the rock	R_d	1.905×10^{-2}	m
Rotational speed	ω	$200 - 1000$	rpm
Density of the fluid	ρ	1×10^{3}	$\mathrm{kg\,m^{-3}}$
Viscosity of the fluid	μ	1×10^{-3}	$\mathrm{Pa\,s}$
Diffusion coefficient of Ca^{2+}	D_0	7.1×10^{-10}	$\mathrm{m^2\,s^{-1}}$
Schmidt number	Sc	1.41×10^{3}	

Table 1: The physical parameters for the reaction vessel, the fluid flow and the dissolution of Ca^{2+} ions.

between our situation and that of the classical von Kármán case. Namely, the spinning disk does not completely cover the top of the reaction vessel and moreover, it is submerged so there is the possibility that an additional circulation cell could form above the disk, changing the nature of the flow. These differences are significant enough to justify a preliminary analysis of the flow field using a CFD program. For our purposes, we chose the package COMSOL based on its availability. Once the fluid velocity is resolved, it can be coupled to an advection-diffusion equation to describe the dissolving Ca^{2+} ions and from that, the flux of material leaving the carbonate rock.

Figure 7 illustrates the geometry of the idealized apparatus, with the inlet/outlet pipes omitted, so that axisymmetric flow is possible and Table 1 lists physical values[4].

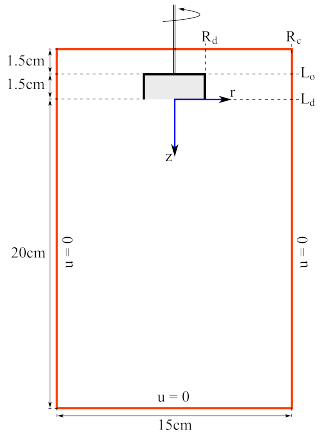

Figure 7: Geometry and boundary conditions for the fluid flow within the idealized reaction vessel.

[4]The value of D_0 comes from [17].

3.2 Velocity field preliminary analysis

The group considered an axisymmetric model for the flow in cylindrical coordinates with the origin located at the disk, the positive direction towards the bottom of the reaction vessel. The fluid flow is assumed to be incompressible and described by the steady state Navier-Stokes equation. It is driven by the motion of the rock and then coupled with an advection-diffusion equation for the transport of Ca^{2+} ions.

In detail, the fluid velocity $\vec{u}(r,z) = (u_r(r,z), u_\theta(r,z), u_z(r,z))$, satisfies

$$u_r\frac{\partial u_r}{\partial r} - \frac{u_\theta^2}{r} + u_z\frac{\partial u_r}{\partial z} = \frac{\mu}{\rho}\left(\frac{1}{r}\frac{\partial}{\partial r}\left(r\frac{\partial u_r}{\partial r}\right) - \frac{u_r}{r^2} + \frac{\partial^2 u_r}{\partial z^2}\right), \tag{11a}$$

$$u_r\frac{\partial u_\theta}{\partial r} + \frac{u_\theta u_r}{r} + u_z\frac{\partial u_\theta}{\partial z} = \frac{\mu}{\rho}\left(\frac{1}{r}\frac{\partial}{\partial r}\left(r\frac{\partial u_\theta}{\partial r}\right) - \frac{u_\theta}{r^2} + \frac{\partial^2 u_\theta}{\partial z^2}\right), \tag{11b}$$

$$u_r\frac{\partial u_z}{\partial r} + u_z\frac{\partial u_z}{\partial z} = -\frac{1}{\rho}\frac{\partial P}{\partial z} + \frac{\mu}{\rho}\left(\frac{1}{r}\frac{\partial}{\partial r}\left(r\frac{\partial u_z}{\partial r}\right) + \frac{\partial^2 u_z}{\partial z^2}\right), \tag{11c}$$

where the pressure $P = P(z)$ is assumed to depend only on the depth and with the incompressibility condition

$$\frac{1}{r}\frac{\partial}{\partial r}(ru_r) + \frac{\partial u_z}{\partial z} = 0. \tag{12}$$

The free surface condition at $z = -L_d$ is assumed to be stress free and all internal surfaces are taken to have a no-slip condition

$$\frac{\partial u_z}{\partial z} = 0, \frac{\partial u_\theta}{\partial z} = 0, u_z = 0; \qquad z = -L_d, \tag{13a}$$

$$\vec{u} = \vec{0}; \qquad z = L_c - L_d, \tag{13b}$$

$$\vec{u} = \vec{0}; \qquad r = R_c, \tag{13c}$$

$$\vec{u} = (0, \omega r, 0); \qquad z = 0, -|L_d - L_0|, \quad 0 < r < R_d, \tag{13d}$$

$$\vec{u} = (0, \omega R_d, 0); \qquad r = R_d, \quad -|L_d - L_0| < z < 0. \tag{13e}$$

Results for the velocity field for $\omega = 50, 100, 200$ rad/s ($477 - 1910$ rpm) are depicted in Figure 8. Note that the axis of symmetry is on the left edge of each plot and that the aspect ratio is not preserved. The existence of the isolated vortex near the wall suggests that sampling near the bottom may lead to fluctuations in measured $[\mathsf{Ca}^{2+}]$. The wall opposite the rotating disk might be a better position to sample the fluid. The structure of the flow has many of the same features of the von Kármán similarity solution despite the fact that the disk is of finite extent and submerged within the fluid.

The thickness of the hydrodynamic or viscous boundary layer under the disk can be estimated by solving for the velocity of the Ekman layer. In a neighbourhood of $z = 0$ this takes the form in cylindrical coordinates of $\vec{u}(z) = u_0 e^{-\lambda z}(\sin\lambda z, \cos\lambda z, 0)$ where $\lambda^2 = \rho\omega/2\mu$. The thickness δ is defined as that depth where $\vec{u}(\delta)/|\vec{u}(\delta)| = -\vec{u}(0)/|\vec{u}(0)|$ or $\lambda\delta = \pi$ so that

$$\delta = \pi\left(\frac{2\mu}{\rho\omega}\right)^{1/2}.$$

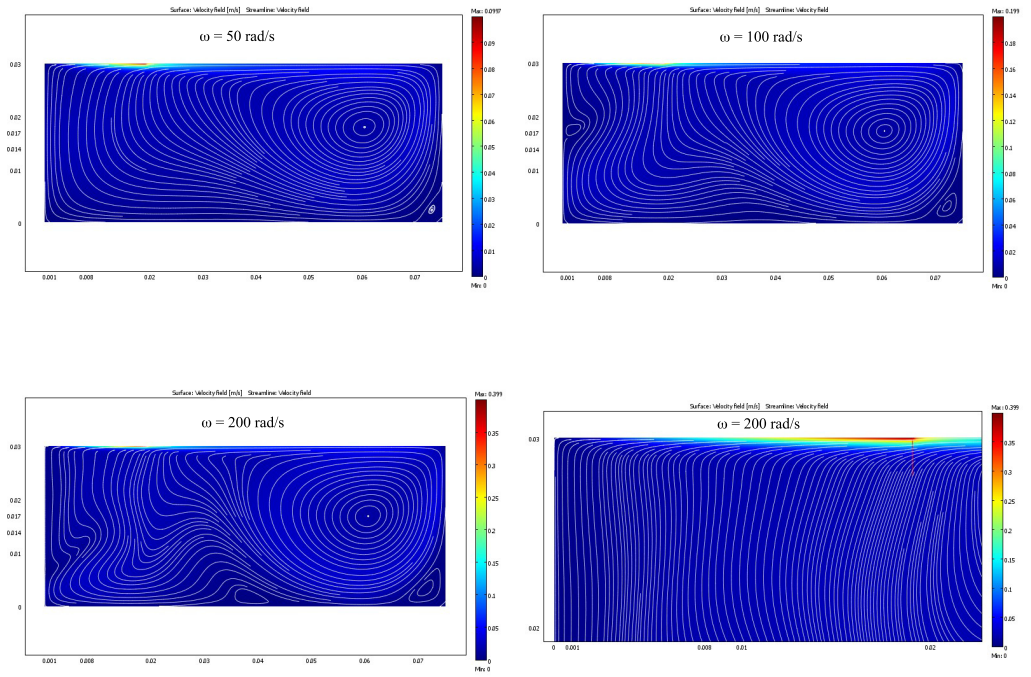

Figure 8: Fluid streamlines for a variety of angular rotation speeds. The figure in the bottom right shows a close up of the fluid flow in the neighbourhood of the disk at 200 rad/s. Only the flow field for $z > 0$ is presented and the aspect ratio has been modified.

Using the values in Table 1 we find a thickness of $\delta = 0.97$ mm at 200 rpm and $\delta = 0.43$ mm at 1000 rpm. Figure 9 shows the change in the angular velocity of the fluid as a function of depth. The hydrodynamic boundary layer is on the order of 1 mm for the rotation speed and over most of the vessel the rotation of the bulk is only 5% of the rotation speed of the disk. This of course assumes laminar flow. Experimental measurements have shown that flow around the disk remains laminar for Reynolds numbers on the order of $\mathrm{Re} = \omega R_d^2 \rho/\mu \sim 2 \times 10^5$ in an axisymmetric vessel [17]. This corresponds to disk rotation speeds of 551 rad/s (5261 rpm) beyond the current upper limit.

3.3 Von Kármán similarity solutions

From the preliminary analysis, the von Kármán similarity solution seems applicable in that (i) near disk, the velocity field is a strong function of radius whereas (ii) far from the spinning disk, the field depended primarily on the depth z. We seek a solution of the form

$$u_r = r\omega h(\xi), \qquad u_\theta = r\omega g(\xi), \qquad u_z = \left(\frac{\mu\omega}{\rho}\right)^{1/2} f(\xi), \qquad P = -\mu\omega\Gamma(\xi) \tag{14}$$

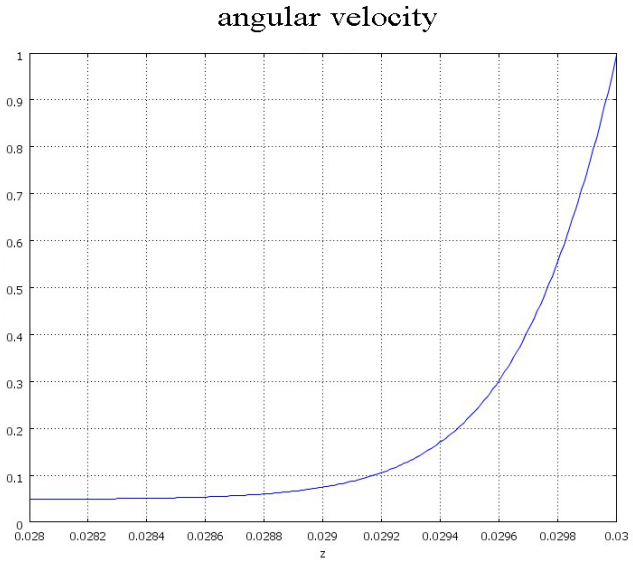

Figure 9: Relative variation of the angular speed with depth in metres showing that the viscous boundary layer is on the order of 1 mm for the rotation speeds of interest. In most of the reaction vessel the speed is only 5% of the rotation speed of the rotating disk.

where $\xi = (\rho\omega/\mu)^{1/2}z$ is nondimensional and of order one within the viscous boundary layer. Substituting (14) into (11) gives the coupled system

$$h^2 - g^2 + h'f = h'', \tag{15a}$$
$$2hg + g'f = g'', \tag{15b}$$
$$ff' = \Gamma' + f'' \tag{15c}$$

and the incompressibility condition reducing to $2h + f' = 0$. Using this last relation to eliminate h gives the system

$$f''' = -\frac{1}{2}f'^2 + 2g^2 + f''f, \tag{16a}$$
$$g'' = -f'g + g'f, \tag{16b}$$
$$\Gamma' = ff' - f''. \tag{16c}$$

At $\xi = 0$, the no-slip condition (13d) gives $f = 0, g = 1$ and $h = 0$. In addition, $f'(0) = 0$, $g'(0) = b$, $h'(0) = -f''(0)/2 = a$ chosen so that as $\xi \to \infty$, $h \to 0, g \to 0$ and $f \to -f_\infty$ corresponding to an upwelling velocity moving towards the disk far outside the boundary layer.

From Levitch [4] and our own numerical simulations, $b = -0.6159286$, $a = 0.5102159$ resulting in $f_\infty \simeq 0.88447$ or $u_z \to -0.88447(\mu\omega/\rho)^{1/2}$. The components of the similarity solution are shown in Figure 10. Having a solution for the velocity in a neighbourhood of the disk we can use this flow field to solve an advection-diffusion equation for the dissolving calcium ions.

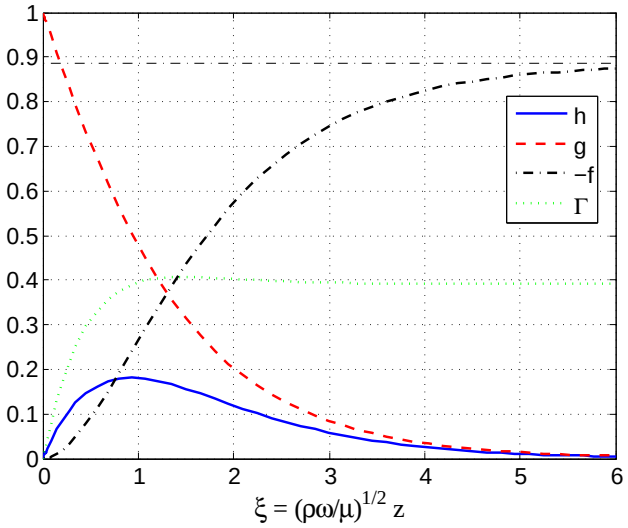

Figure 10: Components of the von Kármán similarity solution as a function of the nondimensional coordinate ξ.

4 Reaction Rate

4.1 Concentration in the diffusive boundary layer

At this point we turn our attention to the advection-diffusion process. We assume that we have a steady process and that there is essentially no variation in concentration radially compared to the axial variation. This results in the expression

$$u_z \frac{\partial c}{\partial z} = D_0 \frac{\partial^2 c}{\partial z^2}.$$

Together with this, we assume that $\lim_{z\to\infty} c(z) = c_b$, the concentration in the bulk, and at the surface of the rock we specify a flux corresponding to a reaction of order n so that

$$D_0 \left.\frac{\partial c}{\partial z}\right|_{z=0} = k c_0^n \tag{17}$$

denoting $c_0 = c(0)$. Using the velocity from the von Kármán solution and scaling the z coordinate with the thickness of the hydrodynamic boundary layer, $\xi = (\rho\omega/\mu)^{1/2} z$, gives the expression

$$f(\xi)\frac{\partial c}{\partial \xi} = \frac{1}{\mathrm{Sc}} \frac{\partial^2 c}{\partial \xi^2}, \tag{18}$$

where $\mathrm{Sc} = \mu/D_0\rho \sim 1.41 \times 10^3 \gg 1$ so there is a boundary layer with thickness $\mathrm{Sc}^{-1/3} \sim 0.089$ in these scaled coordinates. That is, roughly one-tenth the thickness of the viscous boundary layer.

Solving (18) and applying the boundary condition as $\xi \to \infty$ gives

$$c(\xi) = c_0 + (c_b - c_0)\frac{\displaystyle\int_0^{\xi} e^{\int^t \mathrm{Sc}\, f(s)\, ds} dt}{\displaystyle\int_0^{\infty} e^{\int^t \mathrm{Sc}\, f(s)\, ds} dt} \tag{19}$$

with c_0 chosen to satisfy the flux condition (17) at the surface.

4.2 Finding the reaction rate

Having determined the concentration, the rate at which material leaves the rock is the integrated flux over the dissolving surface. Since we have assumed no radial dependence, one has

$$\pi R_d^2 R = \iint_{\text{disk}} D_0 \left.\frac{\partial c}{\partial z}\right|_{z=0} dA = \pi k R_d^2 c_0^n \tag{20a}$$

with

$$c_0^n \int_0^{\infty} e^{\int^t \mathrm{Sc}\, f(s)\, ds} dt = \frac{D_0}{k}\left(\frac{\rho\omega}{\mu}\right)^{1/2}(c_b - c_0). \tag{20b}$$

Traditionally one estimates the integral by replacing $f(\xi)$ with the first term of its Taylor series [4], $f(\xi) \sim -a\xi^2 + O(\xi^3)$ and finds

$$I_\infty(\mathrm{Sc}) = \int_0^{\infty} e^{\int^t \mathrm{Sc}\, f(s)\, ds} dt \sim \left(\frac{a\,\mathrm{Sc}}{3}\right)^{-1/3} \int_0^{\infty} e^{-t^3} dt = \left(\frac{a\,\mathrm{Sc}}{3}\right)^{-1/3} \Gamma\left(\frac{4}{3}\right). \tag{21}$$

Alternatively, if one is already solving the system (15) then

$$I_\infty(\mathrm{Sc}) = \lim_{x\to\infty} I(x;\mathrm{Sc})$$

where $I(x;\mathrm{Sc})$ satisfies $I'' = \mathrm{Sc}\, f(x) I'; I(0) = 0, I'(0) = 1$. Using this technique we find

$$I_\infty(\mathrm{Sc}) \simeq A\mathrm{Sc}^{-\gamma} \tag{22}$$

where $A = 2.08938$, $\gamma = 0.35469$. A comparison of these estimates is shown in Figure 11.

At this point one could solve R as a function of n numerically. Specializing to the case of $n = 1$, equation (20b) gives the approximation

$$c_0 = c_b \left(\left(\frac{a^{1/3}}{3^{1/3}\Gamma(4/3)} \right)^{-1} k D_0^{-2/3} \left(\frac{\mu}{\rho}\right)^{1/6} \omega^{-1/2} + 1 \right)^{-1}$$

leading to the asymptotic expression with respect to ω of

$$R = c_b \begin{cases} \frac{a^{1/3}}{3^{1/3}\Gamma(4/3)} D_0^{2/3} \left(\frac{\mu}{\rho}\right)^{-1/6} \omega^{1/2}, & \omega \to 0, \\ k, & \omega \to \infty. \end{cases} \tag{23}$$

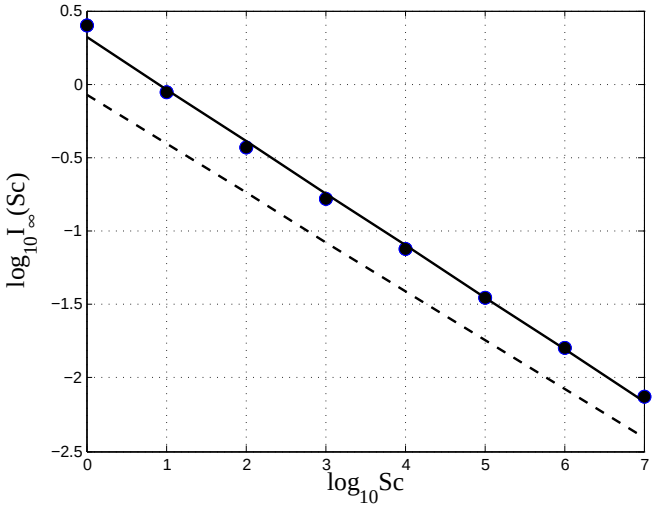

Figure 11: Comparison of the various estimates of $I_\infty(\mathrm{Sc})$. The circles are the actual data points, the solid line is the estimate (22) and the dashed line is the traditional estimate (21).

If expression (22) is used instead then one has

$$R = c_b \begin{cases} A^{-1} D_0^{1-\gamma} \left(\frac{\mu}{\rho}\right)^{\gamma-1/2} \omega^{1/2}, & \omega \to 0, \\ k, & \omega \to \infty. \end{cases} \tag{24}$$

Returning to the traditional estimate, noting that $\frac{a^{1/3}}{3^{1/3}\Gamma(4/3)} = 0.62044$, we see that we have reproduced the original expression (1) given back in Section 1. Also of interest is the case when $c_0 \ll c_b$. In this regime,

$$R = k c_0^n \sim \frac{a^{1/3}}{3^{1/3}\Gamma(4/3)} D_0^{2/3} \left(\frac{\mu}{\rho}\right)^{-1/6} \omega^{1/2} c_b$$

for any order n in contradiction to the expression suggested by Schlumberger.

4.3 A Stefan problem for the Ca^+ dissolution

A simple Stefan problem has been proposed to predict the rate at which calcium carbonate is being dissolved and hopefully to explain the swirling patterns we observed. In this first iteration we ignore the velocity field and assume only diffusion in the bulk. A one dimensional model was taken and assumes that the rock extends from $z = 0$ to $z = S(t)$ with $S(0) = S_0$ being the initial thickness. The solid has some intrinsic concentration which decreases as it is dissolved into the solution and the rate at which this material is lost is taken up in motion of the dissolving interface. The speed of the interface is related to the jump in concentration at the surface. As mentioned, in the bulk of vessel $S(t) < z < L$, the concentration satisfies the diffusion equation (ignoring advection) and a no flux boundary condition is specified at the bottom of the vessel at $z = L$.

Putting all these assumptions together gives the model

$$\begin{aligned}
c(z,t) &= c_s; && 0 \le z < S(t), \quad t \in (0,T] \\
\frac{\partial c}{\partial t} &= D\frac{\partial^2 c}{\partial z^2}; && S(t) < z < L, \quad t \in (0,T] \\
\frac{\partial c}{\partial z} &= 0; && z = L, \quad t \in (0,T]; \\
c(z,t) &= c_0; && z = S(t), \quad t \in (0,T] \\
(c_s - c_0)\frac{dS}{dt} &= D\frac{\partial c}{\partial z}; && z = S(t), \quad t \in (0,T], \quad S(0) = S_0
\end{aligned}$$

where c_s is the concentration of the solid rock and initially we assume some bulk concentration in the solution $c(z,0) = c_b$ for $S_0 < z < L$. T is defined as that time where $S(T) = 0$ and all the material has dissolved. To validate this model it should predict the observed dissolution rate of $dS/dt \sim 3/5$ mm per minute (10^{-5} m s^{-1}).

5 Summary

The flow within the experimental apparatus was modelled and it was found that the Reynolds number varies significantly from the bulk to the layer near the edge of the rotating disk with values from 1000-5000 but the onset of turbulence is not expected until a rotation speed of roughly 5200 rpm. Using COMSOL, the flow was shown to be axisymmetric but in reality it may be more complicated with time dependent behaviour in the corners of the reaction vessel and near the disk. This behaviour will modify the transport of the Ca^{2+} ions which **suggests that a better place to sample the concentration would be away from the bottom of the reaction vessel near the side wall opposite the rotating disk**. One concern is the edge of the disk which was assumed to erode in the modelling described herein. By having material on the edge which does not erode, there is the possibility that a high concentration of ions could be trapped near the surface of the disk, artificially slowing its dissolution. It was proposed that using a material that dissolved might lead to an improvement in the results. The literature on the kinetics of the dissolution of carbonate could be coupled into the model to produce profiles of the concentration of the various chemical species. Details of this nature have so far ignored the advection of the fluid. Another avenue of interest might be to include the porosity of the rock in the Stefan model that was proposed.

Bibliography

[1] Lund, K. et al. (1973). *Acidization I. The Dissolution of Dolomite in Hydrochloric Acid*. Chemical Engineering Science, 28, pp. 691-700.

[2] Lund, K. et al. (1975). *Acidization II. The Dissolution of Calcite in Hydrochloric Acid*. Chemical Engineering Science, 30, pp. 825-835.

[3] Fredd, C.N. & Fogler, H.S. (1998). *The Kinetics of Calcite Dissolution in Acetic Acid Solutions*. Chemical Engineering Science, 53(22), pp. 3863-3874.

[4] Levitch, V.G. (1962). Physicochemical Hydrodynamics, Prentice-Hall Inc., Englewood Cliffs, N.J.

[5] Boomer, D.R. et al. (1972). *Rotating Disk Apparatus for Reaction Rate Studies in Corrosive Liquid Environments*. The Review of Scientific Instruments, 43(2), pp. 225-229.

[6] Newman, J. (1966). *Schmidt Number Corrections for the Rotating Disk*. Journal of Physical Chemistry, 70(4), pp. 1327-1328.

[7] Taylor, K.C. et al. (2004). *Measurement of Acid Reaction Rates of a Deep Dolomitic Gas Reservoir*. Journal of Canadian Petroleum Technology, 43(10), pp. 49-56.

[8] Taylor, K.C. & Nasr-El-Din, H.A. (2009). *Measurement of Acid Reaction Rates with a Rotating Disk Apparatus*. Journal of Canadian Petroleum Technology, 48(6), pp. 66-70.

[9] Prakongpan, S. et al. (1976). *Dissolution Rate Studies of Cholesterol Monohydrate in Bile Acid-Lecithin Solutions Using the Rotating-Disk Method*. Journal of Pharmaceutical Sciences, 65(5), pp. 685-689.

[10] Kármán, T. von. (1921). *Über laminare und turbulente Reibung*. Zeitschrift für Angewandte Mathematik und Mechanik (ZAMM), 1(4), pp. 233-252

[11] Escudier, M.P. (1984). *Observations of the flow produced in a cylindrical container by a rotating endwall*. Experiments in Fluids, 2, pp. 189-196.

[12] Brady, J.F. & Durlofsky, L. (1987). *On rotating disk flow*. Journal of Fluid Mechanics, 175, pp. 363-394.

[13] Hyun, J.M. & Kim, J.W. (1987). *Flow driven by a shrouded spinning disk with axial suction and radial inflow*. Fluid Dynamics Research, 2, pp. 175-182.

[14] Harned, H.S., & Davis, R.D. (1943). *The ionization constant of carbonic acid in water and the solubility of carbon dioxide in water and aqueous salt solutions from* 0 *to* 50^o *C*. Journal of the American Chemical Society, 65(10), pp. 2030-2037.

[15] Harned, H.S., & Scholes, S.R. (1941). *The ionization constant of* HCO_3^- *from* 0 *to* 50^o *C*. Journal of the American Chemical Society, 63(6), pp. 1706-1709.

[16] Dickson, A.G. & Riley, J.P. (1979). *The estimation of acid dissociation constants in seawater media from potentionmetric titrations with strong base. I. The ionic product of water -* K_w. Marine Chemistry, 7(2), pp. 89-99.

[17] Liu, Z. & Dreybrod, W. (1997). *Dissolution kinetics of calcium carbonate minerals in H_2O-CO_2 solutions in turbulent flow: The role of the diffusion boundary layer and the slow reaction $H_2O+ \rightarrow H^+ + HCO_3^-$*. Geochimica et Cosmochimica Acta, 61(14), pp. 2879-2889.

[18] Soli, A.L. & Byrne, R.H. (2002). *CO_2 system hydration and dehydration kinetics and the equilibrium CO_2/H_2CO_3 ratio in aqueous $NaCl$ solution*. Marine Chemistry, 78(2-3), pp. 65-73.

[19] Mucci, A. (1983). *The solubility of calcite and aragonite in seawater at various salinities, temperatures and one atmosphere total pressure*. American Journal of Science, 283, pp. 780-799.